Regulation of Stem Cell Fate in a Three-Dimensional Micropatterned Dual-Crosslinked Hydrogel System

*Oju Jeon and Eben Alsberg**

Micropatterning technology is a powerful tool for controlling the cellular microenvironment and investigating the effects of physical parameters on cell behaviors, such as migration, proliferation, apoptosis, and differentiation. Although there have been significant developments in regulating the spatial and temporal distribution of physical properties in various materials, little is known about the role of the size of micropatterned regions of hydrogels with different crosslinking densities on the response of encapsulated cells. In this study, a novel alginate hydrogel system that can be micropatterned three-dimensionally is engineered to create regions that are crosslinked by a single mechanism or dual mechanisms. By manipulating micropattern size while keeping the overall ratio of single- to dual-crosslinked hydrogel volume constant, the physical properties of the micropatterned alginate hydrogels are spatially tunable. When human adipose-derived stem cells (hASCs) are photoencapsulated within micropatterned hydrogels, their proliferation rate is a function of micropattern size. Additionally, micropattern size dictates the extent of osteogenic and chondrogenic differentiation of photoencapsulated hASC. The size of 3D micropatterned physical properties in this new hydrogel system introduces a new design parameter for regulating various cellular behaviors, and this dual-crosslinked hydrogel system provides a new platform for studying proliferation and differentiation of stem cells in a spatially controlled manner for tissue engineering and regenerative medicine applications.

1. Introduction

Stem cells represent an important cell source in tissue engineering and regenerative medicine due to their high proliferative capacity and ability to differentiate into multiple cell phenotypes under controlled in vitro and in vivo conditions.[1] Over the past couple of decades, major advances have been achieved in the isolation, culture and differentiation of various stem cells, which have been identified in every major organ and tissue of the human body.[2] Mesenchymal stem cells found in many adult tissues, such as bone marrow, fat and muscle, are attractive stem cell sources for the regeneration of damaged tissues because they are able to self-renew with long-term viability and possess the potential to differentiate down several connective tissue lineages.[3,4] In particular, human adipose-derived stem cells (hASCs) can be isolated easily from fat tissue in significant numbers, exhibit stable growth in culture[5,6] and have been shown to be able to differentiate in vitro into osteogenic, adipogenic and chondrogenic cells when treated with established lineage-specific soluble factors.[6] Intense efforts are currently underway to understand the molecular mechanisms underlying the fate decisions of ASCs undergoing self-renewal or differentiation.[7–9] Understanding these mechanisms would help realize the full therapeutic potential of ASCs. However, ASC culture in traditional two-dimensional (2D) culture systems, such as on tissue culture plastic, fails to provide an accurate representation of a physiological ASC microenvironment as it lacks the three-dimensional (3D) biophysical and biochemical cues found in native tissue.[10] Therefore, there are now significant demands for tunable 3D ASC culture systems to address this need. Since stem cell fate is regulated by interactions with neighboring cells, the extracellular matrix (ECM), mechanical signals and soluble factors,[11,12] it is important to have the capacity to control the complexity of these interactions with 3D culture systems.

Micropatterning technology is an important tool for spatially controlling the stem cell microenvironment in biomaterials and investigating the effects of, for example, physical properties of these materials on stem cell behaviors, such as migration, proliferation, apoptosis and differentiation.[13,14] Many approaches based on photolithography,[15] microcontact printing,[16] soft lithography,[17] microfluidics[18] and protein microarrays[19] have been implemented to micropattern surfaces to manipulate the cellular microenvironment. These approaches may allow researchers to study the dynamic responses of stem cells to well-defined model microenvironments and the effects of modulating parameters such as stem cell shape, cell-cell interactions, and cell-extracellular matrix interactions.

Dr. O. Jeon, Prof. E. Alsberg
Department of Biomedical Engineering
Case Western Reserve University
10900 Euclid Ave., Cleveland, OH 44106, USA
E-mail: eben.alsberg@case.edu
Prof. E. Alsberg
Department of Orthopaedic Surgery
Case Western Reserve University
10900 Euclid Ave., Cleveland, OH 44106, USA

DOI: 10.1002/adfm.201300529

© 2013 WILEY-VCH Verlag GmbH & Co. KGaA, Weinheim

Knowledge gained from these studies could lead to new biomaterial design paradigms to control stem cell function and ultimately tissue formation, and thereby further reduce the time required to clinical translation of stem cell-based regenerative therapies.[20,21] Although there have been significant developments in regulating the spatial and temporal distribution of physical properties in various materials, most micropatterning studies in this area have only been applied to surface studies and not for cells in 3D culture conditions, which would better represent the complex spatiotemporal presentation of signals that exist in native tissues.[20]

Hydrogels, which are crosslinked insoluble, hydrophilic 3D networks of water soluble polymers,[22] are attractive biomaterials for use as 3D systems to investigate the role of the extracellular environment on stem cell function because it is possible to precisely tailor their biochemical and physical properties.[23] Only recently have various techniques been used to prepare hydrogels with micropatterned 3D biomaterial properties to examine the influence of stem cell niche signals such as matrix rigidity[24] and topography,[25] growth factors[26–28] and cell adhesion molecules.[26,29] For example, a photopolymerizable hydrogel has been directly micropatterned via photolithography using ultraviolet (UV) light exposure through a photomask to create 3D spatial patterning of rigidity for regulation of human mesenchymal stem cell (hMSC) differentiation.[30] Several groups have utilized microfluidic molding techniques using soft-lithography technology to create micropatterns of matrix elasticity[31] and cell adhesion ligand presentation[32] in hydrogels composed of photopolymerizable synthetic macromers including poly(ethylene glycol)s and functionalized polysaccharides (e.g., chitosan or hyaluronic acid). These methods are simple and robust, and have demonstrated that the creation of micropatterns in 3D cell-laden hydrogels can be useful for investigating stem cell behaviors in response to these spatially-defined cues.

While there have been substantial advances in this area, little is known about the effect of the size of micropatterned regions of hydrogels with different crosslinking densities, which would influence local hydrogel stiffness[33] and transport properties,[34] on encapsulated stem cell growth and differentiation. The purpose of this study was to develop a 3D micropatterned hydrogel system based on oxidized, methacrylated alginate and 8-arm poly(ethylene glycol) amine (OMA/PEG) capable of being crosslinked chemically (single-crosslinked) or chemically and photocrosslinked (dual-crosslinked), and use it to evaluate the effect of micropattern size of hydrogel regions with different crosslinking densities on hASC behavior while keeping the overall ratio of single- to dual-crosslinked hydrogel volume constant. Alginate was functionalized by both oxidation and methacrylation[35] to form dual-crosslinkable hydrogels with a multi-arm PEG. The effects of micropattern size and oxidation degree on the physical properties of bulk hydrogels were evaluated by quantifying swelling and degradation behavior. Additionally, the effect on proliferation and osteogenic, chondrogenic and adipogenic differentiation of photoencapsulated hASCs was examined. This micropatterned dual-crosslinked OMA/PEG hydrogel system may provide a useful platform for studying the role of spatially controlled biomaterial physical properties on the stem cells behavior.

2. Results and Discussion

2.1. Characterization of Micropatterned Dual-crosslinked OMA/PEG Hydrogels

Understanding how microenvironmental factors influence stem cell behaviors is important to inform strategies for tissue engineering.[36] While 3D systems represent more biomimetic microenvironments compared to 2D counterparts, implementation may be hampered by a lack of spatial control over biochemical and biophysical signals.[20] A 3D dual-crosslinked micropatterned hydrogel system was developed in this study to provide a simple and reproducible way to spatially control hydrogel physical properties on the microscale and permit examination of the effect of the size of these hydrogel patterns on encapsulated hASCs behavior. The overall strategy for the formation of the micropatterned dual-crosslinked hydrogels is depicted in **Figure 1**A. The first crosslinked networks were formed by a Schiff base reaction between the aldehyde groups of the OMA and amine groups of the 8-arm PEG (Figure 1B). The second crosslinked networks were formed by photocrosslinking of the methacrylate groups of the OMA in the single-crosslinked OMA/PEG hydrogels thorough photomasks with checkerboard patterns of varying dimensions (Figure 1B). To illustrate the versatility of this approach, a number of dual-crosslinked micropatterned OMA/PEG hydrogels with patterns of various sizes and shapes were prepared. The different micropatterns were visually confirmed using photocrosslinkable methacrylated rhodamine B (Figure 1C) and differential swelling of the hydrogels was demonstrated in water after 1 h incubation (Figure 1D).

The swelling ratio and degradation profile of hydrogels are strongly dependent on the chemical properties of the polymer(s) composing the hydrogels, the network morphology and the interaction between the polymer(s) and the solvent.[37,38] Since the hydrogel swelling affects the transport of oxygen, nutrients and metabolic waste, which are essential for cell survival and growth,[35,39] the overall swelling ratio change of dual-crosslinked micropatterned OMA/PEG hydrogels was investigated relative to checkerboard pattern size and degree of oxidation of alginate. Micropatterned dual-crosslinked OMA/PEG hydrogels were made using alginates with 9, 14 or 20% actual degree of oxidation and 8-arm PEG amines and applying UV light through photomasks with checkerboard tile dimensions of 25, 50, 100, or 200 μm. While the checkerboard dimensions were varied, the ratio of single- to dual-crosslinked hydrogel volume in all of these conditions was 1. Micropatterned dual-crosslinked OMA/PEG hydrogels were allowed to swell in Dulbecco's Modified Eagle Medium (DMEM) at 37 °C, and then the swelling ratio of the swollen mass to the dry mass of hydrogels was calculated and compared at day 1 (**Figure 2**A) and day 14 (Figure 2B). While holding the hydrogel concentration and ratio of single- to dual-crosslinked hydrogel volume constant, the swelling ratio increased significantly with increasing degree of alginate oxidation within each pattern size at both time points, demonstrating that the degree of alginate oxidation had a strong effect on the materials' ability to imbibe and store water within the polymer networks. Interestingly, there was no significant difference in swelling ratio among four different hydrogels at day 1 when micropattern size increased while

© 2013 WILEY-VCH Verlag GmbH & Co. KGaA, Weinheim

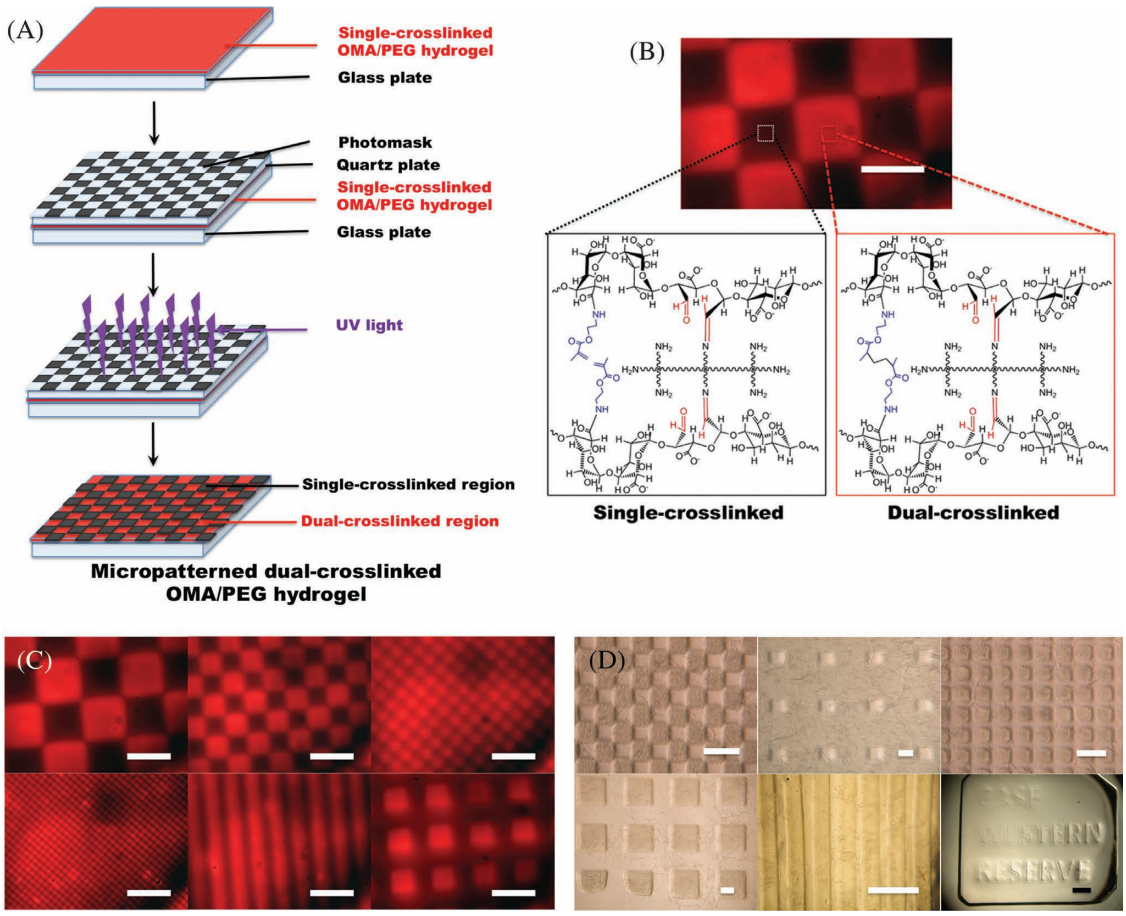

Figure 1. Fabrication of dual-crosslinked micropatterned OMA/PEG hydrogels. A) Schematic illustration of the preparation of a micropatterned dual-crosslinked OMA/PEG hydrogel. B) Fluorescence photomicrograph of a micropatterned dual-crosslinked OMA/PEG hydrogel with a 200 μm checkerboard pattern. The UV blocked regions (dark) consist only of single-crosslinked (chemical) networks formed by Schiff base reaction between the aldehyde groups of the OMA and the amine groups of the 8-arm PEG, whereas the UV exposed regions (red) consist of dual-crosslinked networks formed by chemical crosslinked and photocrosslinked networks. C) Fluorescence and D) optical photomicrographs of micropatterned dual-crosslinked OMA/PEG hydrogels with patterns of various sizes and shapes. The scale bars indicate 200 μm.

holding the oxidation degree constant. After 14 days of incubation, a similar trend of swelling was observed except for 200 μm patterned OMA-9/PEG and OMA-14/PEG hydrogels. The mass loss (%) of dual-crosslinked micropatterned OMA/PEG hydrogels in DMEM at day 14 was determined as a measure of degradation (Figure 2C). Since single-crosslinked OMA/PEG hydrogels completely degraded within 7 days (data not shown) and the volume ratio of single- to dual-crosslinked regions was 1 for all micropatterns, all dual-crosslinked micropatterned OMA/PEG hydrogel exhibited over 50% mass loss at day 14 likely due predominantly to the rapid degradation of the single-crosslinked regions. Due to the higher swelling in OMA-20/PEG hydrogels, the degradation rate of OMA-20/PEG hydrogels was slightly faster than that of the other hydrogels.

2.2. hASC Photoencapsulation within the Micropatterned Dual-crosslinked OMA/PEG Hydrogels

While micropatterning techniques have demonstrated the ability to control stem cell behavior on micropatterned 2D surfaces, controlling organization, growth and differentiation of stem cells in 3D environments still remains a challenge.[20] Here we present a simple, robust approach for controlling the cluster size and growth of hASCs photoencapsulated within 3D micropatterned dual-crosslinked OMA/PEG hydrogels. Cellular morphology of hASCs varied between the single-crosslinked and the dual-crosslinked regions. As shown in **Figure 3**A, hASCs photoencapsulated in the single-crosslinked regions grew into cell clusters, while hASCs encapsulated in the dual-crosslinked regions remained predominantly isolated through 4 weeks. The size of hASC clusters in the single-crosslinked regions depends on the micropattern size, and high cell viability was observed throughout all micropattern sizes for 4 weeks. 3D clusters of cells can sometimes better mimic complex 3D structures and functions of native tissue, which are not easily replicated in conventional 2D culture.[40,41] Several techniques utilizing, for example, hanging drops,[43] non-adhesive surfaces,[44] and roller bottles,[45] have been developed to induce 3D cell cluster formation. However, it is not possible to have precise control over cluster size with these methods. Since cell

© 2013 WILEY-VCH Verlag GmbH & Co. KGaA, Weinheim

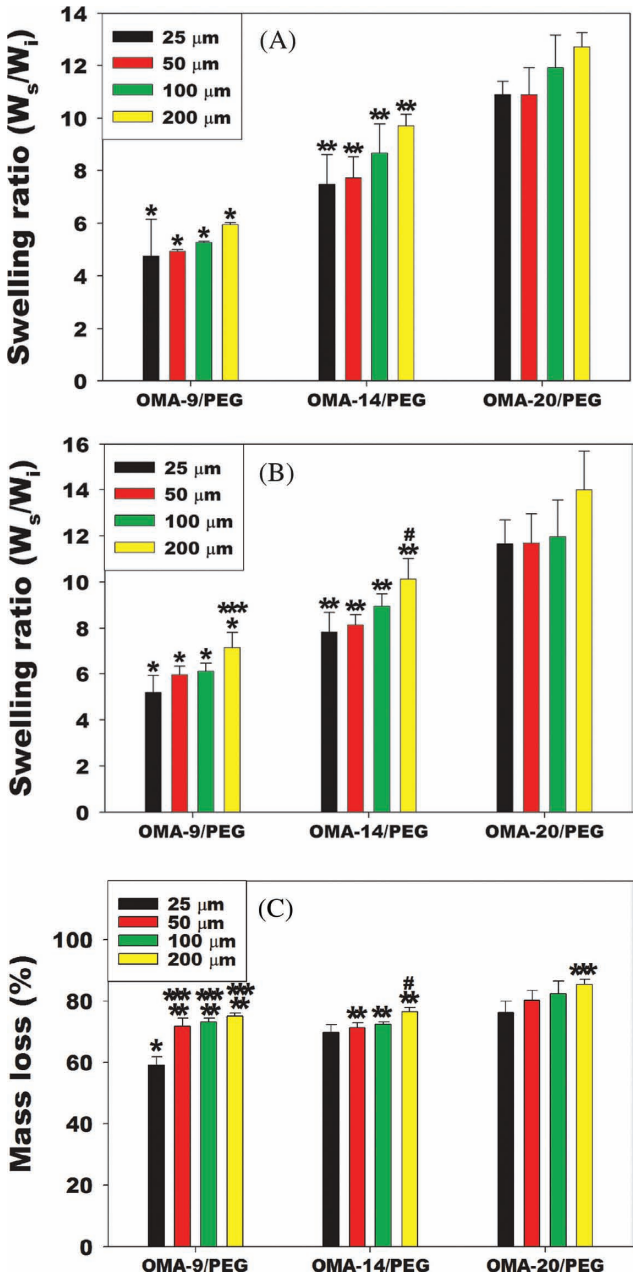

Figure 2. Swelling ratio and degradation in vitro. Swelling ratios of micropatterned dual-crosslinked OMA/PEG hydrogels with checkerboard patterns of different dimensions (25, 50, 100, and 200 μm) and oxidation degrees at A) day 1 and B) day 14. C) Mass loss of micropatterned dual-crosslinked OMA/PEG hydrogels at day 14. $^{*}p < 0.05$ compared with OMA-14/PEG and OMA-20/PEG at the same pattern size. $^{**}p < 0.05$ compared with OMA-20/PEG at the same pattern size. $^{***}p < 0.05$ compared with 25 μm at the same oxidation level. $^{\#}p < 0.05$ compared with 25 and 50 μm at the same oxidation level.

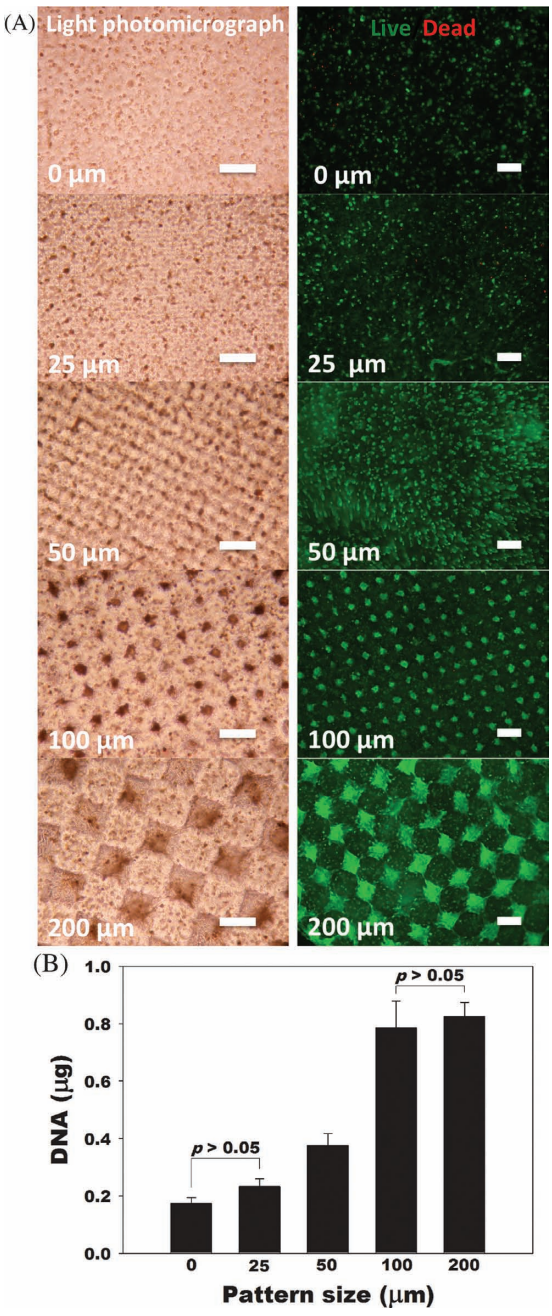

Figure 3. Micropatterning of hASCs for regulating cellular organization. A) Representative optical and Live (FDA, green)/Dead (EB, red) photomicrographs of hASCs photoencapsulated in micropatterned dual-crosslinked OMA/PEG hydrogels after 4 weeks culture in vitro. All scale bars indicate 200 μm. B) Quantification of DNA in the constructs. $p<0.05$, unless indicated otherwise in figure.

behaviors such as differentiation and proliferation are known to be affected by cell cluster size[42] and uncontrolled cluster growth could induce cell necrosis in the core, these strategies could be problematic in 3D cluster formation.[40] Recently, microwell cell culture platforms using microfabrication techniques have been developed to create precisely controlled cell clusters.[40,46,47] In these systems, cells are allowed to passively settle within microwell via sedimentation. These cell clusters can then be removed from the microwells and encapsulated within biomaterials for further implantation or applications.[47] Regulating both cluster formation and location directly

© 2013 WILEY-VCH Verlag GmbH & Co. KGaA, Weinheim

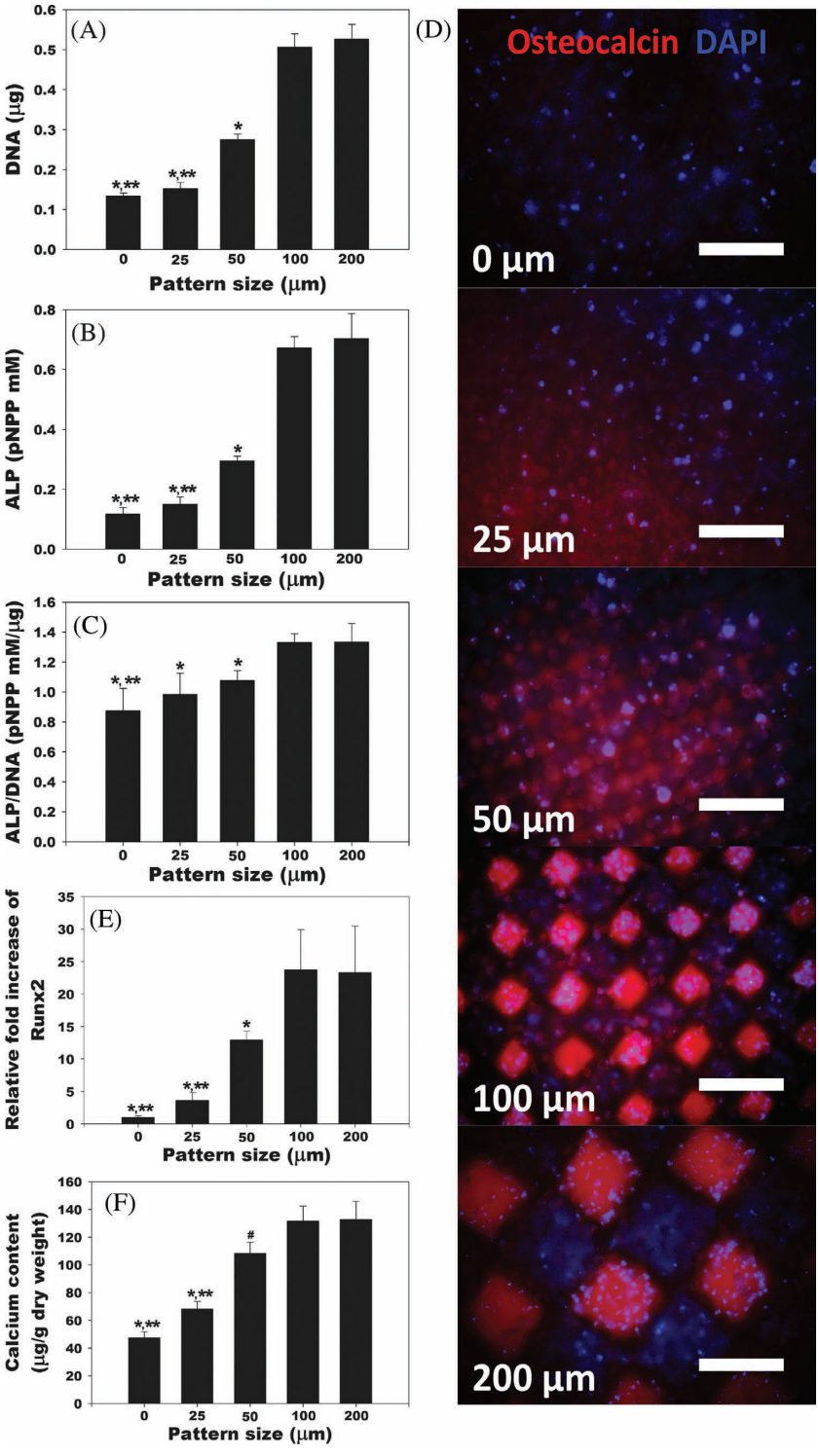

Figure 4. Quantification of A) DNA, B) ALP, and C) ALP/DNA. D) Representative fluorescence photomicrographs of hASCs photoencapsulated in micropatterned dual-crosslinked OMA/PEG hydrogels stained for osteocalcin (red) and nuclei (DAPI, blue) after culture in osteogenic differentiation media for 4 weeks. All scale bars indicate 200 μm. E) Relative runt-related transcription factor-2 (Runx2) gene expression and F) calcium content in the constructs. The relative gene expression levels were normalized using the control unpatterned (0 μm) group. $^{*}p < 0.05$ compared with 100 and 200μm, $^{**}p < 0.05$ compared with 50 μm, and $^{\#}p < 0.05$ compared with 200 μm

within a hydrogel has not been previously reported. In this study, the use of micropatterned dual-crosslinked OMA/PEG hydrogels for hASC encapsulation yielded relatively uniform cell clusters, which scaled in size with micropatterned checkerboard dimensions. As the dimensions of the unit square in the checkerboards increased form 25 to 200 μm, a corresponding increase in cluster size was oberved (Figure 3A). The growth of photoencapsulated hASCs was also controllable. As the micropatterned checkerboard size increased from 25 to 100 μm, the overall number of encapsulated hASCs increased as determined by DNA content assay (Figure 3B). The larger patterns resulted in larger cell clusters in the single-crosslinked regions, and the increased cell-cell interactions may have promoted cell proliferation.[48,49] Since a simple yet robust method that provides precise control over 3D stem cell cluster size has not previously been demonstrated, the micropatterned dual-crosslinked OMA/PEG hydrogel developed in this study could be a useful platform to investigate the effect of cell cluster size on the behavior of stem cells, such as embryonic stem cells, MSCs and induced pluripotent stem cells. For example, the dimensions of embryoid bodies (EBs) have been shown to be a crucial factor in controlling embryonic stem cell differentiation,[46] therefore a straightforward system for reliably creating controlled sizes of EBs in a 3D hydrogel niche could be of great value to understanding embryonic stem cell fate decisions.

2.3. Osteogenic, Chondrogenic, and Adipogenic Differentiation of Photoencapsulated hASCs in Micropatterned Hydrogels

To investigate the effect of micropattern size on stem cell fate, hASCs photoencapsulated within micropatterned dual-crosslinked hydrogels were first cultured in osteogenic differentiation media for 4 weeks. Cell/hydrogel constructs were evaluated for hASC osteogenic differentiation by measuring alkaline phosphatase (ALP) activity, immunostaining for osteocalcin, determining relative mRNA expression of Runt-related transcription factor 2 (Runx2), and quantifying calcium deposition (**Figure 4**). As the micropattern size increased, the ASC proliferation and ALP activity, an early osteogenic differentiation marker, of cell-hydrogel constructs increased as determined by measuring DNA content (Figure 4A) and

© 2013 WILEY-VCH Verlag GmbH & Co. KGaA, Weinheim

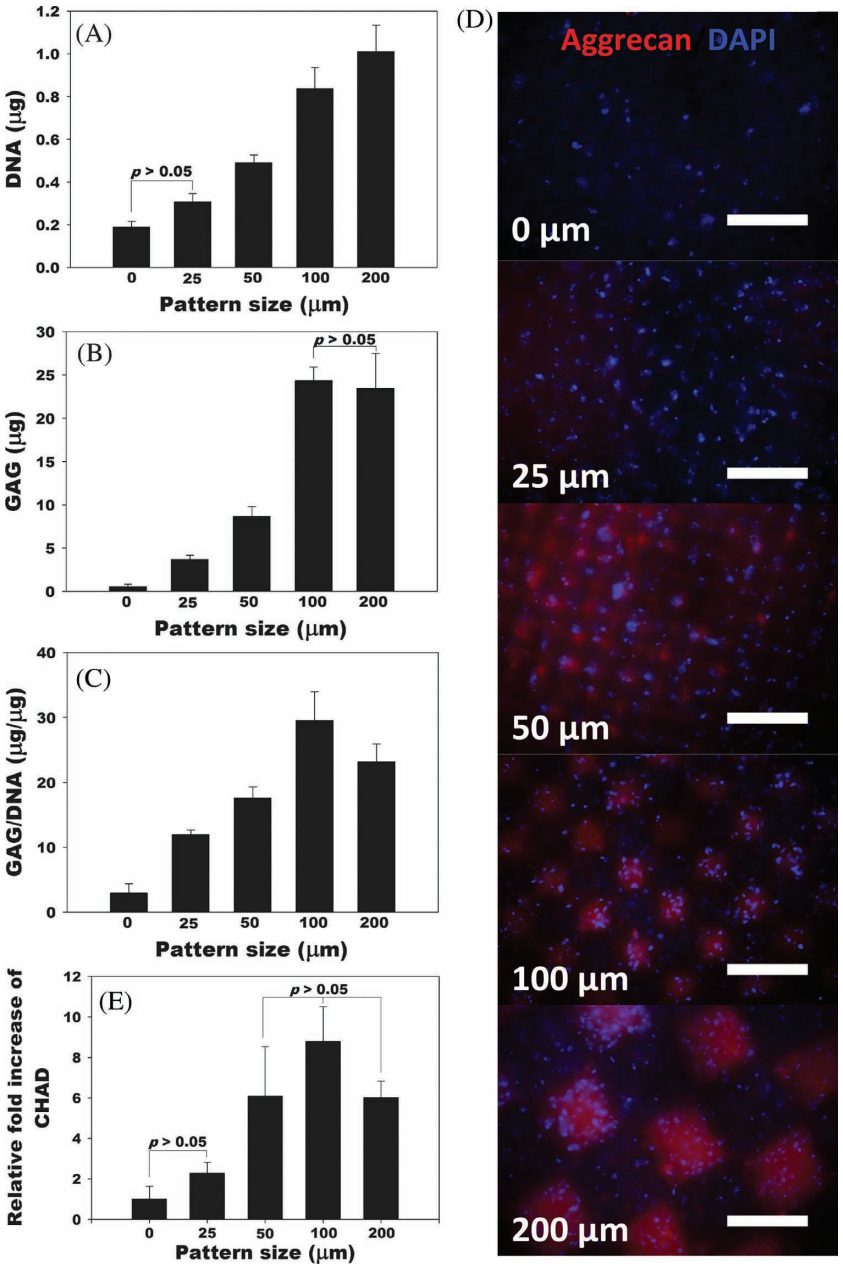

Figure 5. Quantification of A) DNA, B) GAG, and C) GAG/DNA. D) Representative fluorescence photomicrographs of hASCs photoencapsulated in micropatterned dual-crosslinked OMA/PEG hydrogels stained for aggrecan (red) and nuclei (DAPI, blue) after culture in chondrogenic differentiation media for 4 weeks. All scale bars indicate 200 μm. E) Relative chondroadherin (CHAD) gene expression in the constructs. The relative gene expression levels were normalized using the control unpatterned (0 μm) group. $p < 0.05$, unless indicated otherwise in figures.

conversion of p-nitrophenylphosphate (pNPP) to 4-Nitrophenol (Figure 4B), respectively. Interestingly, it was found that when hASCs encapsulated in hydrogels with larger pattern sizes (100 and 200 μm), the ALP activity, which was normalized by DNA content, was higher compared to smaller pattern sizes (25 and 50 μm) and the no pattern control group. (Figure 4C). Since the ALP can be expressed by other differentiated cells,[50] it is important to examine other osteogenic differentiation markers as well. Therefore, immunohistostaining for osteocalcin and a quantitaive analysis of mRNA expression levels of Runx2 by real-time quantitative reverse transcription-polymerase chain reaction (qRT-PCR) were performed. Compared to the no pattern dual-crosslinked group, more intense red osteocalcin staining was observed in the micropatterned dual-crosslinked hydrogel groups. Moreover, the intensity of the staining signal increased as the micropattern size increased up to 100 μm (Figure 4D). Since the ultimate indicator of stem cell osteogenic differentiation is calcium deposition,[51] the calcium content in the cell-hydrogel contructs was also quantified. Similar to the other osteogenic markers, calcium deposition increased with increasing micropattern size, with the highest calcium content in the dual-crosslinked micropatterned hydrogels with 100 and 200 μm pattern sizes. These results demonstrate that the variation of micropattern size in these dual-crosslinked 3D hydrogels is a strong regulator for the osteogenic differentiation of the photoencapsulated stem cells. Changing the micropattern size locally changes the size of hydrogel regions with specific crosslinking densities and therefore physical properties (e.g., swelling, mechanical, degradation, etc.), and this in turn influences the capacity of the cells to form clusters which may influence their proliferation and osteogenic differentiation. The enhanced cluster formation and differentiation occurs in the single-crosslinked regions; this is potentially due to the lower mechanical properties, increased swelling and more rapid degradation of these regions which could provide more space for cell-cell interactions, proliferation and extracellular matrix production.[39,52,53] It is important to reiterate that the ratio of single- to dual-crosslinked hydrogel volume in all of the micropatterned hydrogels was 1, so the differences observed can be attributed directly to differences in pattern size.

hASCs photoencapsulated within micropatterned dual-crosslinked hydrogels were also cultured in chondrogenic differentiation media for 4 weeks to determine the effect of pattern size on chondrogenesis. Cell/hydrogel constructs were evaluated by quantifying glycosaminoglycan (GAG) content, immunostaining for aggrecan, and measuring relative mRNA expression of chondroadherin (CHAD) (**Figure 5**). Similar to the osteogenic differentiation findings, the ASC proliferation, as determined by measuring DNA, and GAG content of cell-hydrogel constructs increased as the micropattern size increased (Figure 5A,B). Even after normalization, the GAG/DNA values increased with increasing size of micropattern up to 100 μm (Figure 5C). To

© 2013 WILEY-VCH Verlag GmbH & Co. KGaA, Weinheim

visualize the chondrogenic ECM expressed by chondrogenically differentiated hASCs encapsulated in the micropatterned dual-crosslinked hydrogels, immunostaining for aggrecan, which is a differentiation marker of chondrocytes and one of the main components of cartilage ECM, was performed. As shown in Figure 5D, the aggrecan expression of hASCs gradually increased as the micropattern size increased. A quantitative analysis of mRNA expression of chondroadherin (CHAD), which is a mature chondrocyte marker,[54] in the constructs further confirmed this correlation (Figure 5D). From these results, pattern sizes 100 μm or greater may be optimal for chondrogenic differentiation of hASCs encapsulated in micropatterned dual-crosslinked OMA/PEG hydrogels. These results parallel those for osteogenesis in that they demonstrate that variation of micropattern size in the 3D hydrogel system can also regulate chondrogenic differentiation of the ASCs.

The effect of micropattern size on adipogenic differentiation of the stem cells was then assessed. The photoencapsulated hASCs within micropatterned dual-crosslinked OMA/PEG hydrogels were cultured in adipogenic differentiation media for 4 weeks. Cell/hydrogel contructs were evaluated by immunostaining and measuring relative mRNA expression of fatty acid binding protein-4 (FABP-4), commonly known as an adipogenic differentiation marker (**Figure 6**). Even though more FABP-4 positive staining signal was observed in the micropatterned dual-crosslinked hydrogels (Figure 6B–E) compared to the no pattern control group (Figure 6A), there was no significant difference of relative FABP-4 mRNA expression of hASCs among any of the pattern sizes as determined by qRT-PCR (Figure 6F). These results indicate that 3D adipogenic differentiation of the ASCs photoencapsulated in dual-crosslinked OMA/PEG hydrogels may not be as strongly influenced by the presence of the micropattern.

Since cell-cell interactions play a key role in differentiation of stem cells,[55] it was examined whether micropattern size of hydrogels had any effect on the cell-cell interactions of encapsulated hASCs by F-actin/vinculin immunostaining and quantifying human cadherin 1 (CDH1) mRNA expression using qRT-PCR (**Figure 7**). The clusters of hASCs formed extensive cell networks with cell-cell junctions as demonstrated by multiple points of adhesion with neighboring cells visualized with F-actin/vinculin staining,[56,57] while hASCs encapsulated in control dual-crosslinked hydrogels without micropatterning (0 μm) remained rounded and predominantly isolated without spreading (Figure 3A). As the micropattern size increased from 25 to 200 μm, F-actin/vinculin expression of hASCs encapsulated in micropatterned dual-crosslinked OMA/PEG hydrogels increased. Additionally, cell-cell interactions, as measured by relative CDH1 mRNA expression of hASCs in micropatterned hydrogels, with the 50, 100, and 200 μm patterns was significantly higher than that of the OMA/PEG hydrogels without micropatterning or the 25 μm pattern. Since the osteogenic and chondrogenic differentiation of photoencapsulated hASCs in dual-crosslinked OMA/PEG hydrogels increased with increasing micropattern size as indicated in Figure 4 and Figure 5, these results indicate that cell-cell interactions afford a potent cue of osteogenic and chondrogenic differentiation of hASCs in the hydrogels, and may be a critical design parameter for tissue engineering approaches. The dual-crosslinking system presented here provides a promising system for spatially regulating hydrogel properties, cell-cell clustering interactions, and ultimately stem cell differentiation.

3. Conclusions

In this study, we have engineered a novel alginate/PEG hydrogel system that could be micropatterned three-dimensionally by a single mechanism or dual mechanisms to spatially control hydrogel physical properties on the microscale and permit examination of the effect of the size of these hydrogel patterns on encapsulated stem cell behavior. By manipulating micropattern size while keeping the overall ratio of single- to dual-crosslinked hydrogel volume constant, the physical properties of the micropatterned alginate hydrogels were spatially tunable. When hASCs were photoencapsulated within micropatterned hydrogels, their viability was high and proliferation rate was a function of micropattern size. Additionally, micropattern size dictated the extent of osteogenic and chondrogenic differentiation of photoencapsulated hASC. The control of the size of 3D micropatterned physical properties in this new hydrogel system introduces a new design parameter for regulating various cellular behaviors, and this dual-crosslinked hydrogel system provides a novel platform for studying proliferation and differentiation of stem cells in a spatially controlled manner for understanding the role of defined microenvironmental signals on cell function and tissue engineering applications.

4. Experimental Section

Microfabrication of Micropatterned, Dual-Crosslinked OMA/PEG Hydrogels: The OMA macromers were prepared as previously described.[35] Details on the preparation of OMAs are presented in the Supporting Information. Eight-arm PEG-amine hydrochloric acid salt (8-arm PEG amine/HCl, 20 g, Mw = 10 000 Da, Jenkem Technology USA Inc., Allen, TX) was dissolved in 100 mL methylene chloride (Fisher Scientific, Pittsburgh, PA), and triethylamine (the mole ratio of triethylamine to HCl of 8-arm PEG amine/HCl = 2, Fisher Scientific) was added into the PEG solution to remove HCl salt from the 8-arm PEG amine/HCl. After 24 h, the solution was precipitated into excess of hexanes (Fisher Scientific), dried under reduced pressure, and rehydrated to a 10% (w/v) solution in ultrapure deionized water (diH_2O) for further purification. The 8-arm PEG amines were further purified by dialysis against diH_2O (MWCO 3500; Spectrum Laboratories Inc., Rancho Dominguez, CA) for 3 days, filtered (0.22 μm filter) and lyophilized. OMA (20% w/v) and 8-arm PEG amines (40% w/v) were separately dissolved in DMEM (Sigma, St. Louis, MO) with 0.05% w/v photoinitiator [2-hydroxy-4'-(2-hydroxyethoxy)-2-methylpropiophenone, Irgacure-2959, Sigma]. To create a single-crosslinked hydrogel, OMA solution (250 μL) was placed in one 1 mL syringe, and an equal volume of 8-arm PEG amine solution was placed in a second 1 mL syringe. The two solutions were mixed for 1 min by joining the syringes together with a Luer-Lok connector. Immediately after mixing the two solutions, the resultant mixture was injected between quartz (top) and glass (bottom) plates separated by 0.4 mm spacers, and incubated for 30 min to form a single-crosslinked hydrogel. Subsequently, a photomask was placed on top of the quartz plate, and a micropatterned dual-crosslinked hydrogel was formed by exposure to UV light 15 cm away (320–500 nm, EXFO OmniCure S1000-1B, Lumen Dynamics Group, Mississauga, Ontario, Canada) at ≈1 mW/cm^2 through the photomask for 5 min. Fluorescent hydrogels were prepared with methacryloxyethyl

© 2013 WILEY-VCH Verlag GmbH & Co. KGaA, Weinheim

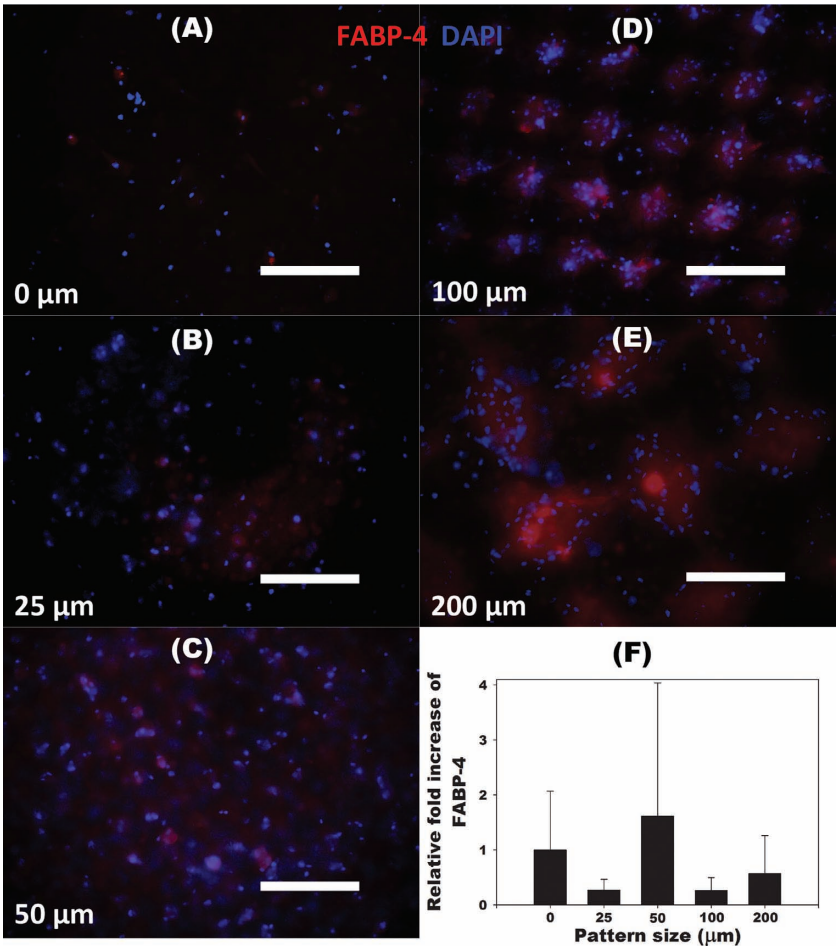

Figure 6. A–E) Representative fluorescence photomicrographs of hASCs photoencapsulated in micropatterned dual-crosslinked OMA/PEG hydrogels stained for fatty acid binding protein-4 (FABP-4, red) and nuclei (DAPI, blue) after culture in adipogenic differentiation media for 4 weeks. All scale bars indicate 200 µm. F) Relative FABP-4 gene expression in the constructs. The relative gene expression levels were normalized using the control unpatterned (0 µm) group.

thiocarbamoyl rhodamine B (0.01% w/v, Polysciences Inc., Warrington, PA) mixed into the macromer solution. Since it is a photocrosslinkable dye, the methacryloxyethyl thiocarbamoyl rhodamine B was covalently incorporated only into the dual-crosslinked regions that were exposed to the UV light, and the uncrosslinked fluorophore from the single-crosslinked regions was removed by extracting and washing the hydrogels for 1 h. The zonal distribution of single and dual-crosslinked regions in the micropatterned dual-crosslinked hydrogels was visualized using fluorescence microscopy (ECLIPSE TE 300, Nikon, Tokyo, Japan) equipped with a digital camera (Retiga-SRV, Qimaging, Burnaby, BC, Canada). By using photomasks with checkerboard patterns of different dimensions (25, 50, 100, and 200 µm), micropatterned dual-crosslinked hydrogels with different pattern sizes that mirrored the photomasks were generated. Micropatterned hydrogel disks were created using a 6 mm diameter biopsy punch. Dual-crosslinked OMA/PEG hydrogel without photomask (0 µm) served as a control group.

Swelling and Degradation of Micropatterned, Dual-Crosslinked OMA/PEG Hydrogels: The micropatterned dual-crosslinked hydrogels were lyophilized and dry weights (W_i) were measured. Dried samples were immersed in 50 mL of DMEM and incubated at 37 °C to reach equilibrium swelling state for 24 h, and the weight of swollen hydrogel samples (W_s) were measured. Samples were immersed again in 50 mL of DMEM and incubated at 37 °C, and the DMEM was replaced after 7 days. After 14 days, samples were removed, rinsed with fresh DMEM, and the swollen (W_s) hydrogel sample weights were measured again. The swelling ratio (Q) was calculated by $Q = W_s/W_i$. After weighing the swollen hydrogel samples, the samples were lyophilized and weighed (W_d). The percent mass loss was calculated by $(W_i - W_d)/W_i \times 100$.

Fabrication of Cell-Laden Micropatterned Dual-Crosslinked Hydrogels: hASCs were isolated from the adipose tissue using a previously reported method.[58] Briefly, lipoaspirates were digested with 200 unit/mg collagenase type I (Worthington Biochemical Products, Lakewood, NJ) for 40 min at 37 °C. The stromal fraction was then isolated by density centrifugation and the stromal cells were plated at 3500 cells/cm^2 on tissue culture plastic in DMEM/F12 (BioWhittaker, Suwance, GA) with 10% defined fetal bovine serum (FBS, HyClone, Logan, UT), 100 U/ml penicillin and 100 µg/mL streptomycin (1% P/S, BioWhittaker). hASCs at passage 1 were cryopreserved in liquid nitrogen in medium containing 80% FBS, 10% DMEM, and 10% dimethylsulfoxide (Sigma). Upon thawing, hASCs were expanded by plating at 8000 cells/cm^2 in DMEM/F12 containing 10% FBS, 1% P/S (Gibco, Grand Island, NY), and 100 ng/mL recombinant human fibroblast growth factor-2 (R&D Systems, Minneapolis, MN). hASCs at passage 3 were photoencapsulated in the micropatterned dual-crosslinked OMA-14/PEG hydrogels by suspension in macromer solution with 0.05% w/v photoinitiator. The micropatterned dual-crosslinked hydrogel construct disks (6 mm diameter) were prepared as previously described using macromer solutions containing hASCs (5×10^6 cells/mL). hASC/dual-crosslinked hydrogel constructs without using a photomask (0 µm) served as controls. Disks were placed in 24-well tissue culture plates with 1 mL of growth media (AdvanceSTEM Mesenchymal Stem Cell Basal Medium containing 10% FBS, Thermo Scientific, Waltham, MA), osteogenic differentiation media (AdvanceSTEM Mesenchymal Stem Cell Osteogenic Differentiation Medium containing 10% FBS, Thermo Scientific), chondrogenic differentiation media (AdvanceSTEM Mesenchymal Stem Cell Chondrogenic Differentiation Medium containing 10% FBS, Thermo Scientific), or adipogenic differentiation media (AdvanceSTEM Mesenchymal Stem Cell Adipogenic Differentiation Medium containing 10% FBS, Thermo Scientific) and cultured in a humidified incubator at 37 °C with 5% CO_2 with gentle shaking for 4 weeks with medium changed every three days.

Biochemical Assay Analysis of Cell-Laden Micropatterned Dual-Crosslinked Hydrogels: The viability and morphology of photoencapsulated hASCs in the micropatterned dual-crosslinked hydrogels were examined using a Live/Dead assay comprised of fluorescein diacetate (FDA, Sigma) and ethidium bromide (EB, Sigma).[38] 20 µL of staining solution was added into each well and incubated for 3–5 min at room temperature, and then stained hydrogel-cell constructs were imaged using a fluorescence microscope with a digital camera.

After 4 weeks of culture, some hydrogel-cell constructs cultured in osteogenic differentiation media were removed from media, homogenized at 35 000 rpm for 30 s using a TH homogenizer (Omni International, Marietta, GA) and lysed by repeated sample freezing and thawing three times, and the lysates were cleared by centrifugation at 16 200*g* for 10 min using a microcentrifuge (accuSpin Micro 17R, Fisher Scientific). After centrifuging, supernatant (100 µL) was mixed with 1×Tris-EDTA buffer (100 µL, Invitrogen, Carlsbad, CA) containing

© 2013 WILEY-VCH Verlag GmbH & Co. KGaA, Weinheim

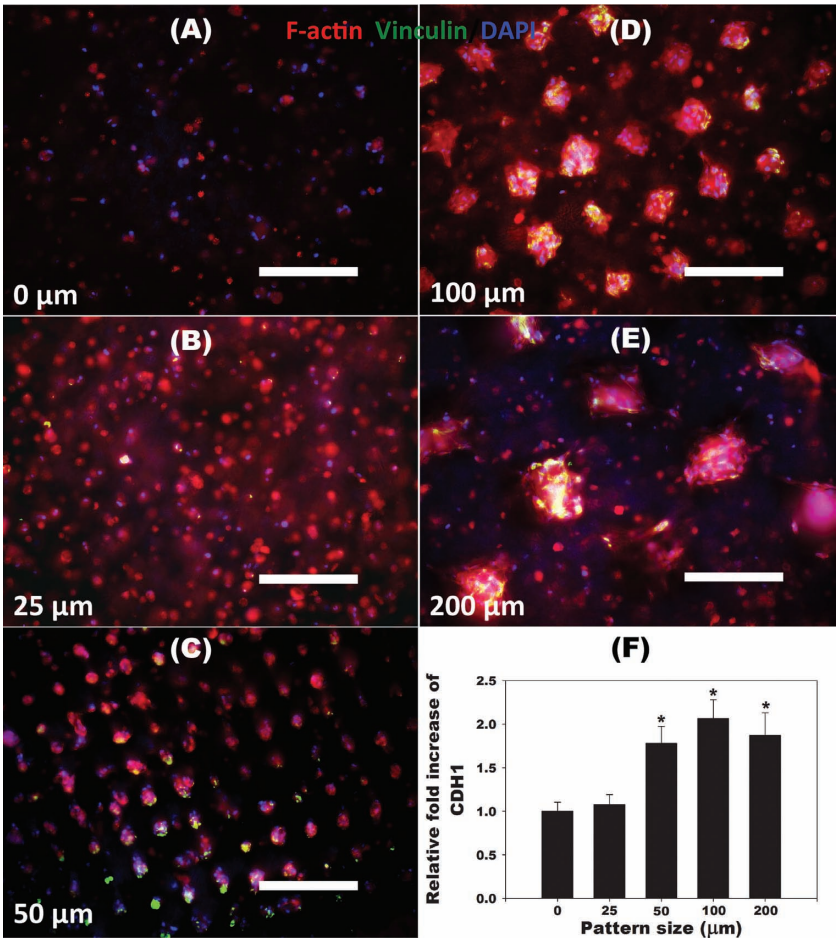

Figure 7. A–E) Representative fluorescence photomicrographs of hASCs photoencapsulated in micropatterned dual-crosslinked OMA/PEG hydrogels stained for F-actin (red), vinculin (green) and nuclei (DAPI, blue) after 4 weeks culture in vitro. All scale bars indicate 200 µm. F) Relative cadherin 1, type 1, E-cadherin (epithelial) (CDH1) gene expression of hASCs photoencapsulated in micropatterned dual-crosslinked OMA/PEG hydrogels after culture in DMEM containing 10% FBS for 4 weeks. The relative gene expression levels were normalized using the control unpatterned (0 µm) group. $^{*}p < 0.05$ compared with 0 and 25 µm.

fluorescent PicoGreen reagent (Invitrogen) and incubated at room temperature for 30 min. Fluorescence intensity of the dye-conjugated DNA solution was measured in 96-well plates on a plate reader (480 nm excitation and 520 nm emission, SAFIRE, Tecan, Austria), and the DNA content was calculated from a standard curve generated with calf thymus DNA (Invitrogen). The ALP activity of hASCs photoencapsulated in the hydrogels was measured using an ALP Assay kit (Sigma, Saint Louis, MO) according to the manufacturer's instructions. Supernatant (25 µL) was incubated with ALP substrate containing pNPP (150 µL, Sigma) at 37 °C for 30 min. The reaction was stopped by addition of 3 N NaOH (25 µL) to the substrate reaction solution. The absorbance of the samples was read at 405 nm on a plate reader and compared with a standard curve prepared with 4-nitrophenol standard solution (Sigma). Each ALP activity measurement was normalized to DNA content.

After 4 weeks of culture, some hydrogel-cell constructs cultured in chondrogenic differentiation media were removed from media, homogenized at 35000 rpm for 30 seconds using a TH homogenizer (Omni International) and digested in 1 mL papain buffer solution (25 µg/mL papain, Sigma, 2 mM L-cysteine, Sigma, 50 mM sodium phosphate, Sigma, 2 mM ethylenediaminetetraacetic acid, Fisher Scientific, at pH 6.5 in nuclease-free water, Ambion, Austin, TX) at 65 °C overnight. After centrifugation of papain-digested samples at 16 200*g* for 10 min, the DNA content of photoencapsulated hASCs in the micropatterned dual-crosslinked hydrogels was quantified as described earlier. GAG content was measured using the standard dimethylmethylene blue (DMMB, Sigma) assay[59] in 96-well plates. In each well, supernatant (50 µL) was mixed with dye (250 µL) containing 16 mg/L DMMB and 3.04 g/L glycine (pH 1.5, Sigma). The absorbance was read at 595 nm using the plate reader. Chondroitin-6-sulfate (Sigma) from shark cartilage was used to construct the standard curve.

Immunofluorescent Staining: To visualize the cytoskeleton structure and focal adhesions of photoencapsulated hASCs in the micropatterned dual-crosslinked hydrogels, filamentous actin (F-actin), vinculin, and nuclei were stained with an actin cytoskeleton/focal adhesion stain kit (Millipore, Billerica, MA). Hydrogel-cell constructs were fixed with 4% paraformaldehyde for 40 min, permeabilized with 0.1% Triton X-100 for 10 min, and blocked with 1% BSA in PBS for 1 h. For immunostaining of focal adhesions, samples were incubated in mouse anti-vinculin monoclonal primary antibody for 2 h at room temperature, followed by incubation with FITC-conjugated goat anti-mouse IgG secondary antibody (Millipore) for 2 h at room temperature. For double-staining of all F-actin, rhodamine-conjugated phalloidin (Millipore) was incubated simultaneously with the secondary antibody. Nuclear counterstaining was performed by incubation with 4′,6-diamidino-2-phenylindole (DAPI, Millipore) to visualize the cell nucleus, and then stained hydrogel-cell constructs were imaged using a fluorescence microscope with a digital camera.

To visualize the osteogenic, chondrogenic and adipogenic differentiation of hASCs photoencapsulated in micropatterned dual-crosslinked OMA/PEG hydrogels, fluorescence immunostaining of osteocalcin, aggrecan and FABP-4 was performed using the hMSC functional identification kit (SC006, R&D Systems) according to the manufacture's protocol. Nuclear counterstaining was also performed by incubation with DAPI, and then stained hydrogel-cell constructs were imaged using fluorescence microscopy with a digital camera.

RNA Isolation and qRT-PCR: RNA was isolated from hydrogel-cell constructs with TRI Reagent (Sigma), and first-strand cDNA was synthesized with Superscript III reverse transcriptase (Invitrogen) according to the manufacturer's instructions. qRT-PCR was performed with 2× SYBR Green Master Mix (Applied Biosystems, Foster City, CA) according to the manufacturer's instructions. The primer sequences used for qRT-PCR are in **Table 1**. All reactions were run on an ABI 7700 Real-Time PCR instrument (Applied Biosystems) with 2 min at 50 °C and 10 min at 95 °C followed by 40 cycles of a two-step thermocycling program: 15 s denaturing at 95 °C, 1 min annealing/extension at 60 °C. Results were analyzed with SDS software (Applied Biosystems) and the RQ (relative quantity) Manager Software (Applied Biosystems) for automated data analysis. Relative expression for the target gene of interest (TGI) was normalized to GAPDH using the delta threshold cycle (ΔCt) method.[60] Namely, the Ct for each gene and endogenous control GAPDH in each sample were used to create a ΔCt_{TGI} value (Ct_{TGI}-Ct_{GAPDH}). Thereafter, ΔΔCt values were calculated by subtracting the ΔCt_{TGI} of the control (0 µm) from the ΔCt_{TGI} of experimental groups (25, 50, 100, and 200 µm checkerboard). The relative expression of target gene was calculated using the equation; $2^{-\Delta\Delta Ct}$.

© 2013 WILEY-VCH Verlag GmbH & Co. KGaA, Weinheim

Table 1. Primer sequences used for qRT-PCR

Gene	Direction	Primer sequeence	Size [bp]	Accession number
GAPDH	Forward	GAGTCAACGGATTTGGTCGT	158	NM_002046
	Reverse	TTGATTTTGGAGGGATCTCG		
Runx2	Forward	CAAACAACCACAGAACCACA	245	NM_001024630
	Reverse	CCCAAAAGAAGTTTTGCTGA		
CHAD	Forward	AGCTCTCTCACAACCCTCTG	228	NM_007689
	Reverse	GGTTGTTGGTGAGAGTGAGG		
FABP-4	Forward	TCACTGCAGATGACAGGAAA	165	NM_001442
	Reverse	AAACTCTCGTGGAAGTGACG		
CDH1	Forward	TGCTCTTGCTGTTTCTTCGG	423	NM_004360.2
	Reverse	TGCCCCATTCGTTCAAGTAG		

Statistical Analysis: All quantitative data is expressed as mean ± standard deviation (N = 3). Statistical analysis was performed with one-way analysis of variance (ANOVA) with Tukey significant difference post hoc test using Origin software (OriginLab Co., Northampton, MA, USA). A value of $p < 0.05$ was considered statistically significant.

Supporting Information

Supporting Information is available from the Wiley Online Library or from the author.

Acknowledgements

The authors would like to thank Dr. Jeffrey Gimble for providing the hASCs. The authors gratefully acknowledge funding from the National Institute of Arthritis And Musculoskeletal And Skin Diseases of the National Institutes of Health under Award Number R01AR061265 and the National Institute of Dental & Craniofacial Research of the National Institutes of Health under Award Number R56DE022376. The contents of this publication are solely the responsibility of the authors and do not necessarily represent the official views of the National Institutes of Health.

Received: February 8, 2013
Revised: March 5, 2013
Published online: April 11, 2013

[1] A. J. Engler, S. Sen, H. L. Sweeney, D. E. Discher, *Cell* **2006**, *126*, 677.
[2] C. Chai, K. W. Leong, *Mol. Ther.* **2007**, *15*, 467.
[3] M. Korbling, Z. Estrov, *N. Engl. J. Med.* **2003**, *349*, 570.
[4] M. F. Pittenger, A. M. Mackay, S. C. Beck, R. K. Jaiswal, R. Douglas, J. D. Mosca, M. A. Moorman, D. W. Simonetti, S. Craig, D. R. Marshak, *Science* **1999**, *284*, 143.
[5] P. A. Zuk, M. Zhu, H. Mizuno, J. Huang, J. W. Futrell, A. J. Katz, P. Benhaim, H. P. Lorenz, M. H. Hedrick, *Tissue Eng.* **2001**, *7*, 211.
[6] J. Gimble, F. Guilak, *Cytotherapy* **2003**, *5*, 362.
[7] L. Ma, Y. Yang, S. C. Sikka, P. J. Kadowitz, L. J. Ignarro, A. B. Abdel-Mageed, W. J. Hellstrom, *Proc. Natl. Acad. Sci. USA* **2012**, *109*, 2090.
[8] R. P. Zhang, J. Z. Shao, L. X. Xiang, *J. Biol. Chem.* **2011**, *286*, 41083.
[9] J. A. Cho, H. Park, E. H. Lim, K. W. Lee, *J. Genet.* **2011**, *90*, 81.
[10] R. James, S. G. Kumbar, C. T. Laurencin, G. Balian, A. B. Chhabra, *Biomed. Mater.* **2011**, *6*, 025011.
[11] B. M. Baker, C. S. Chen, *J. Cell. Sci.* **2012**, *125*, 3015.
[12] B. T. Estes, J. M. Gimble, F. Guilak, *Stem Cells. Dev. Dis.* **2004**, *60*, 91.
[13] S. Gobaa, S. Hoehnel, M. Roccio, A. Negro, S. Kobel, M. P. Lutolf, *Nat. Methods* **2011**, *8*, 949.
[14] X. Shi, S. Chen, J. Zhou, H. Yu, L. Li, H. Wu, *Adv. Funct. Mater.* **2012**, *22*, 3799.
[15] N. Li, C. M. Ho, *Lab Chip* **2008**, *8*, 2105.
[16] R. Peerani, K. Onishi, A. Mahdavi, E. Kumacheva, P. W. Zandstra, *PLoS One* **2009**, *4*, e6438.
[17] D. Qin, Y. Xia, G. M. Whitesides, *Nat. Protoc.* **2010**, *5*, 491.
[18] E. Tenstad, A. Tourovskaia, A. Folch, O. Myklebost, E. Rian, *Lab Chip* **2010**, *10*, 1401.
[19] L. Ceriotti, L. Buzanska, H. Rauscher, I. Mannelli, L. Sirghi, D. Gilliland, M. Hasiwa, F. Bretagnol, M. Zychowicz, A. Ruiz, S. Bremer, S. Coecke, P. Colpo, F. Rossi, *Soft Matter* **2009**, *5*, 1406.
[20] A. W. Lund, B. Yener, J. P. Stegemann, G. E. Plopper, *Tissue Eng., Part B* **2009**, *15*, 371.
[21] B. Murtuza, J. W. Nichol, A. Khademhosseini, *Tissue Eng., Part B* **2009**, *15*, 443.
[22] H. Geckil, F. Xu, X. H. Zhang, S. Moon, U. Demirci, *Nanomedicine* **2010**, *5*, 469.
[23] G. D. Nicodemus, S. J. Bryant, *Tissue Eng., Part B* **2008**, *14*, 149.
[24] R. A. Marklein, J. A. Burdick, *Soft Matter* **2010**, *6*, 136.
[25] M. Diez, V. A. Schulte, F. Stefanoni, C. F. Natale, F. Mollica, C. M. Cesa, J. Y. Chen, M. Moller, P. A. Netti, M. Ventre, M. C. Lensen, *Adv. Eng. Mater.* **2011**, *13*, B395.
[26] R. G. Wylie, S. Ahsan, Y. Aizawa, K. L. Maxwell, C. M. Morshead, M. S. Shoichet, *Nat. Mater.* **2011**, *10*, 799.
[27] J. E. Leslie-Barbick, C. Shen, C. Chen, J. L. West, *Tissue Eng., Part A* **2011**, *17*, 221.
[28] S. S. Shah, M. Kim, K. Cahill-Thompson, G. Tae, A. Revzin, *Soft Matter* **2011**, *7*, 3133.
[29] R. Peng, X. Yao, J. D. Ding, *Biomaterials* **2011**, *32*, 8048.
[30] S. Khetan, J. A. Burdick, *Biomaterials* **2010**, *31*, 8228.
[31] T. Rossow, J. A. Heyman, A. J. Ehrlicher, A. Langhoff, D. A. Weitz, R. Haag, S. Seiffert, *J. Am. Chem. Soc.* **2012**, *134*, 4983.
[32] J. H. Slater, J. S. Miller, S. S. Yu, J. L. West, *Adv. Funct. Mater.* **2011**, *21*, 2876.
[33] L. Bian, C. Hou, E. Tous, R. Rai, R. L. Mauck, J. A. Burdick, *Biomaterials* **2013**, *34*, 413.
[34] Y. H. Hu, J. O. You, D. T. Auguste, Z. G. Suo, J. J. Vlassak, *J. Mater. Res.* **2012**, *27*, 152.

© 2013 WILEY-VCH Verlag GmbH & Co. KGaA, Weinheim

[35] O. Jeon, D. S. Alt, S. M. Ahmed, E. Alsberg, *Biomaterials* **2012**, *33*, 3503.
[36] Y. B. Sun, C. S. Chen, J. P. Fu, *Annu. Rev. Biophys.* **2012**, *41*, 519.
[37] S. Chaterji, I. K. Kwon, K. Park, *Prog. Polym. Sci.* **2007**, *32*, 1083.
[38] O. Jeon, K. H. Bouhadir, J. M. Mansour, E. Alsberg, *Biomaterials* **2009**, *30*, 2724.
[39] K. T. Nguyen, J. L. West, *Biomaterials* **2002**, *23*, 4307.
[40] D. Gallego-Perez, N. Higuita-Castro, S. Sharma, R. K. Reen, A. F. Palmer, K. J. Gooch, L. J. Lee, J. J. Lannutti, D. J. Hansford, *Lab Chip* **2010**, *10*, 775.
[41] F. Grinnell, W. M. Petroll, *Annu. Rev. Cell Dev. Biol.* **2010**, *26*, 335.
[42] E. Eschbach, S. S. Chatterjee, M. Noldner, E. Gottwald, H. Dertinger, K. F. Weibezahn, G. Knedlitschek, *J. Cell. Biochem.* **2005**, *95*, 243.
[43] J. Kramer, P. Schlenke, J. Rohwedel, *Curr. Protoc. Cell Biol.* **2007**, *23*, 5.
[44] Y. Hori, I. C. Rulifson, B. C. Tsai, J. J. Heit, J. D. Cahoy, S. K. Kim, *Proc. Natl. Acad. Sci. USA* **2002**, *99*, 16105.
[45] C. Shiba, T. Daikoku, F. Goshima, H. Takakuwa, Y. Yamauchi, O. Koiwai, Y. Nishiyama, *J. Gen. Virol.* **2000**, *81*, 2397.
[46] Y. S. Hwang, B. G. Chung, D. Ortmann, N. Hattori, H. C. Moeller, A. Khademhosseini, *Proc. Natl. Acad. Sci. USA* **2009**, *106*, 16978.
[47] A. B. Bernard, C. C. Lin, K. S. Anseth, *Tissue Eng., Part C* **2012**, *18*, 583.
[48] C. M. Nelson, C. S. Chen, *FEBS Lett.* **2002**, *514*, 238.
[49] W. F. Liu, C. M. Nelson, D. M. Pirone, C. S. Chen, *J. Cell Biol.* **2006**, *173*, 431.
[50] B. F. Hinnebusch, A. Siddique, J. W. Henderson, M. S. Malo, W. Y. Zhang, C. P. Athaide, M. A. Abedrapo, X. M. Chen, V. W. Yang, R. A. Hodin, *Am. J. Physiol.: Gastrointest. Liver Physiol.* **2004**, *286*, G23.
[51] J. Lock, H. N. Liu, *Int. J. Nanomed.* **2011**, *6*, 2769.
[52] S. J. Bryant, J. L. Cuy, K. D. Hauch, B. D. Ratner, *Biomaterials* **2007**, *28*, 2978.
[53] R. A. Marklein, J. A. Burdick, *Adv. Mater.* **2010**, *22*, 175.
[54] Z. X. Shen, S. Gantcheva, B. Mansson, D. Heinegard, Y. Sommarin, *Biochem. J.* **1998**, *330*, 549.
[55] S. S. Chen, W. Fitzgerald, J. Zimmerberg, H. K. Kleinman, L. Margolis, *Stem Cells* **2007**, *25*, 553.
[56] H. W. Kaiser, W. Ness, I. Jungblut, R. A. Briggaman, H. W. Kreysel, E. J. O'Keefe, *J. Invest. Dermatol.* **1993**, *100*, 180.
[57] G. M. Sumida, T. M. Tomita, W. Shih, S. Yamada, *BMC Cell Biol.* **2011**, *12*, 48.
[58] B. T. Estes, B. O. Diekman, J. M. Gimble, F. Guilak, *Nat. Protoc.* **2010**, *5*, 1294.
[59] B. O. Enobakhare, D. L. Bader, D. A. Lee, *Anal. Biochem.* **1996**, *243*, 189.
[60] K. J. Livak, T. D. Schmittgen, *Methods* **2001**, *25*, 402.

© 2013 WILEY-VCH Verlag GmbH & Co. KGaA, Weinheim